Letter

Efficient time-dependent dynamics of matrix product states using average Hamiltonians

Belal Abouraya,[1,2] Jirawat Saiphet,[3] Fedor Jelezko,[2,*] and Ressa S. Said[2,4,†]

[1]*Laboratory of Micro-optics, Faculty of Information Engineering and Technology, German University in Cairo (GUC), 11865 Cairo, Egypt*
[2]*Institute for Quantum Optics and Center for Integrated Quantum Science and Technology, Universität Ulm, 89081 Ulm, Germany*
[3]*Institut für Theoretische Physik, Eberhard Karls Universität Tübingen, 72076 Tübingen, Germany*
[4]*XeedQ GmbH, Wilhelm-Runge-Straße 10/3, 89081 Ulm, Germany*

(Received 28 January 2026; accepted 6 October 2026; published 18 November 2026)

Simulating quantum many-body systems (QMBS) is one of the long-standing, highly nontrivial challenges in condensed matter physics and quantum information due to the exponentially growing size of the system's Hilbert space. To date, tensor networks have been an essential tool for studying such quantum systems, owing to their ability to efficiently capture the entanglement properties of the systems they represent. One of the well-known tensor network architectures, namely, matrix product states (MPS), is the standard method for simulating one-dimensional QMBS. Here, we propose a simple, yet efficient, method to augment the already available MPS algorithms to simulate the dynamics of time-dependent Hamiltonians with better accuracy and a faster convergence rate, giving a second-order convergence compared to the first-order convergence of the Riemann method available in standard software packages. We apply our proposed method to simulate the dynamics of a chain of single spins associated with nitrogen-vacancy (NV) color centers in diamond, which has potential applications for practical and scalable quantum technologies, and find that our method improves the average error for a system of a few NV centers by a factor of about 1000 for moderate step sizes. Additionally, we compare our method to the midpoint rule, which has second-order convergence as well, and show some of the trade-offs between the two methods. Our work paves the way for efficient simulation of QMBS under the influence of time-dependent Hamiltonians.

DOI: 10.1103/cxv4-r2bs

Introduction. Since the inception of the density matrix renormalization group [1] and its subsequent interpretation as the variational optimization of matrix product states (MPS) [2], tensor networks (TNs) have become a key element in studying quantum many-body systems (QMBS), on account of their efficiency, accuracy, and scalability. Despite the fact that development of TNs for two or more dimensions is still elusive, they offer a wide range of well-developed methods for one-dimensional (1D) and quasi-1D systems. Many TN representations exist, for instance, multiscale entanglement renormalization ansatz, matrix product states (MPS), projected entangled pair states, and tree tensor networks. Up to now, the MPS, also known as *the tensor train decomposition*, is the most well-established representation [1–5], with a variety of methods for simulating QMBS under time-independent Hamiltonians, such as the time-evolving block decimation (TEBD) and matrix product operator (MPO) W^{II} [2–5]. However, the principal challenge in investigating QMBS numerically is the dynamical simulation governed by time-dependent Hamiltonians that describe many physical phenomena, such as those typically found in quantum control and spectroscopy using external time-dependent driving fields [6,7], in Floquet Hamiltonian engineering of many-body systems [8], and in open quantum system dynamics approximated by time-dependent effective Hamiltonians [9]. While a recent treatment [10] attempted to address this using an alternative to established trotterization-based methods, it yielded improved results only for systems with fast driving fields and introduced significant implementation overhead.

Our work presented in this Letter is to address the above-mentioned challenge and motivated by the need for a simple-yet-highly efficient way to improve the existing MPS time-evolution solvers, or *time steppers*, and to maintain their higher-order accuracies. We substitute the instantaneous Hamiltonian used inside the fixed-order MPS time steppers by a carefully chosen average Hamiltonian, which is computed from a high-order quadrature rule. This approach leverages classical numerical integration ideas based on Simpson's rules to better approximate the time-evolution operator over a short time interval. It is analytically simple and directly applicable to the existing MPS time-evolution solvers, for instance, TEBD. Therefore, our method requires only a minimal change to the TN's standard numerical libraries. Our numerical simulations demonstrate the method's improved performance, where improvement factors of up to 200 and 4000 in the average error are observed when simulating systems of two and three spins, respectively, when compared with the standard Riemann stepper. The spins are associated with negatively charged nitrogen-vacancy (NV) color centers in diamond

*Contact author: fedor.jelezko@uni-ulm.de
†Contact author: ressa@xeedq.com

Published by the American Physical Society under the terms of the Creative Commons Attribution 4.0 International license. Further distribution of this work must maintain attribution to the author(s) and the published article's title, journal citation, and DOI.

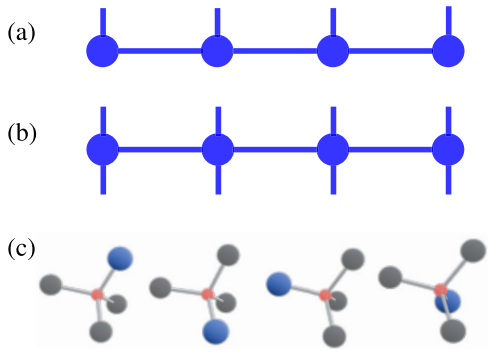


FIG. 1. (a) One-dimensional tensor networks of a quantum state, and (b) the corresponding Hamiltonian representation. (c) A chain of nitrogen-vacancy color centers in diamond. The blue and red spheres represent a pair of nitrogen and vacancy, tetrahedrally coordinated in the carbon lattice having an axial trigonal C_{3V} symmetry. The negatively charged NV (denoted simply as the NV throughout the Letter) has an extra electron located at the vacancy site forming a spin ($S = 1$) pair with one of the vacancy electrons, and therefore inducing spin triplet ground states. The spin chain is due to nearest-neighbor interactions of dipolar coupling (not shown in the figure), where each spin can have one out of four different quantization axes.

(see Fig. 1). The NV systems are chosen as our simulation platform owing primarily to their remarkable physical properties that are promising for various quantum technology applications operating at ambient temperature, such as quantum registers [11] and quantum sensors [12,13]. For a larger system size of NVs, our method shows a steady improvement in the average error by a factor of approximately 50 compared with the Riemann method.

The time evolution. Simulating the dynamics of a quantum system governed by the time-dependent Schrödinger equation comes down to computing the time evolution of the quantum state $|\psi\rangle$, following

$$|\psi(\Delta t)\rangle = U(\Delta t)|\psi(0)\rangle; \tag{1}$$

for a sufficiently small time step Δt, we can assume that the Magnus expansion converges and the evolution operator $U(\Delta t)$ can be expressed as

$$U(\Delta t) = \exp(\Omega(\Delta t)), \tag{2}$$

where $\Omega(\Delta t)$ is the Magnus expansion of $-iH(\Delta t)$ [14].

For MPS, computing the time evolution can be divided into two broad classes. The first class approximates the effect of the evolution operator directly on the MPS, without computing the operator itself. Meanwhile, the second class approximates the evolution operator first and then efficiently applies it to the MPS [4]. Here, we are mainly concerned with the second class of methods by focusing on the second-order TEBD and second-order complex time-step MPO W^{II} algorithms [15,16]. These methods are uniquely characterized as they can approximate the evolution operator for a constant Hamiltonian with a third-order error for a single step, giving a second-order error for multiple steps in the constructed unitary. For a time-independent Hamiltonian, a third-order algorithm will yield an operator

$$\widetilde{U}(\Delta t, H) = \exp(-i\Delta t H) + O(\Delta t^3) = U(\Delta t) + O(\Delta t^3). \tag{3}$$

However, this is valid only for a time-independent Hamiltonian. For the time-dependent case, one can use a simple time stepper, *the Riemann stepper*, which has been available in the standard TN libraries, such as TenPy [17]. It works by substituting the value of the Hamiltonian in the left end point of the time interval into the time-evolution method of choice. Starting with

$$H_{\mathrm{Riem}}(\Delta t) := H(0) \tag{4}$$

and using this construction in a third-order algorithm yields

$$\widetilde{U}_{\mathrm{Riem}}(\Delta t, H) := \widetilde{U}(\Delta t, H_{\mathrm{Riem}}) = U(\Delta t) + O(\Delta t^2). \tag{5}$$

Alternatively, one may consider substituting an average Hamiltonian into the algorithm construction to obtain the new evolution operator. Here, we propose the average Hamiltonian in the form of

$$H_{\mathrm{Simp}}(\Delta t) := \tfrac{1}{6}(H(0) + 4H(\Delta t/2) + H(\Delta t)), \tag{6}$$

which makes use of Simpson's integration rule to construct a new time-evolution operator that retains the same error bound. Hence, the new constructed operator is

$$\widetilde{U}_{\mathrm{Simp}}(\Delta t, H) := \widetilde{U}(\Delta t, H_{\mathrm{Simp}}(\Delta t)) = U(\Delta t) + O(\Delta t^3). \tag{7}$$

To examine the validity of the error bounds, we provide the proof for the generic error bound that is subsequently used for the specific integrators. Here, we use $\|\cdot\|$, to denote the Hölder-∞ norm of a matrix and assume two matrices $A(\Delta t)$ and δ, having $\|\delta\| = O(\Delta t^k)$. Starting with Eq. (11.16.8), p. 694, of Ref. [18], we obtain

$$e^{A(\Delta t)+\delta} = e^{A(\Delta t)} + \int_0^1 e^{(1-\tau)A(\Delta t)} \delta e^{\tau(A(\Delta t)+\delta)} d\tau. \tag{8}$$

Now, using Eq. (11.15.7 (xiv)), p. 690, of Ref. [18], we arrive at

$$\begin{aligned} \|e^{A(\Delta t)+\delta} - e^{A(\Delta t)}\| &= \left\| \int_0^1 e^{(1-\tau)A(\Delta t)} \delta e^{\tau(A(\Delta t)+\delta)} d\tau \right\| \\ &\leqslant \int_0^1 \left\| e^{(1-\tau)A(\Delta t)} \delta e^{\tau(A(\Delta t)+\delta)} \right\| d\tau \\ &\leqslant \int_0^1 \|e^{(1-\tau)A(\Delta t)}\| \|\delta\| \|e^{\tau(A(\Delta t)+\delta)}\| d\tau \end{aligned} \tag{9}$$

and

$$\begin{aligned} \|e^{A(\Delta t)+\delta} - e^{A(\Delta t)}\| &\leqslant \int_0^1 e^{(1-\tau)\|A(\Delta t)\|} \|\delta\| e^{\|\tau(A(\Delta t)+\delta)\|} d\tau \\ &\leqslant \int_0^1 e^{(1-\tau)\|A(\Delta t)\|} \|\delta\| e^{\|\tau A(\Delta t)\| + \|\tau\delta\|} d\tau \\ &= \int_0^1 e^{\|A(\Delta t)\|} \|\delta\| e^{\|\tau\delta\|} d\tau. \end{aligned} \tag{10}$$

Assuming $\|A(t)\|$ is bounded by M, for $t \geqslant 0$, we now have

$$\begin{aligned}\|e^{A(\Delta t)+\delta} - e^{A(\Delta t)}\| &\leqslant e^M \int_0^1 \|\delta\|(1+\tau\|\delta\|+\cdots)d\tau \\ &\leqslant e^M \int_0^1 O(\Delta t^k)(1+\tau O(\Delta t^k))d\tau \\ &= O(\Delta t^k). \end{aligned} \tag{11}$$

Finally notice that since the Simpson rule is symmetric about the midpoint of the interval, it approximates the Magnus expansion to the third order (see p. 92 of Ref. [14]). Namely,

$$\Omega(\Delta t) = -i\Delta t H_{\text{Simp}}(\Delta t) + O(\Delta t^3). \tag{12}$$

Using this last equation with Eqs. (2), (3), and (11), one gets

$$\begin{aligned}\widetilde{U}_{\text{Simp}}(\Delta t, H) &= \exp(\Omega(\Delta t) + O(\Delta t^3)) + O(\Delta t^3) \\ &= U(\Delta t) + O(\Delta t^3). \end{aligned} \tag{13}$$

The Riemann rule, however, only approximates the first term of the expansion, giving

$$\Omega(\Delta t) = -i\Delta t H_{\text{Riem}}(\Delta t) + O(\Delta t^2). \tag{14}$$

Using the same reasoning as above, we get

$$\begin{aligned}\widetilde{U}_{\text{Riem}}(\Delta t, H) &= \exp(\Omega(\Delta t) + O(\Delta t^2)) + O(\Delta t^3) \\ &= U(\Delta t) + O(\Delta t^2). \end{aligned} \tag{15}$$

Numerical simulations. We numerically investigate our proposed time-evolution method to simulate a chain of N spin-1 ($S = 1$) sites with nearest-neighbor interactions (Fig. 1), subject to an external driving pulse, representing a typical system of N NV centers driven by a microwave (MW) pulse.

In the frame rotating with the MW frequency and using the conventional rotating-wave and secular approximations, the system Hamiltonian is modeled by [11,19] (here we set $\hbar = 1$, and use the unit in 2π)

$$H = H^{\text{drift}} + u(t) \times H^{\text{control}}, \tag{16}$$

where

$$\begin{aligned} H^{\text{drift}} &= \bigotimes_{j=1}^{N} H_j^0 + H^{\text{int}}, \\ H_j^0 &= (D-\omega_0)S_{z,j}^2 - \gamma_e B_{z,j} S_{z,j}, \\ H^{\text{int}} &= \sum_{j=1}^{N-1} g_j S_{z,j} S_{z,j+1}, \\ H^{\text{control}} &= \frac{1}{2}\sum_{j=1}^{N} S_{x,j}. \end{aligned} \tag{17}$$

Here, the parameter D is the NV center zero-field splitting energy, while γ_e is the associated electronic gyromagnetic ratio of the NV spin. $B_{z,j}$ denotes the z component of the magnetic field bias experienced by the j th NV center. The coupling strength between neighboring NV centers is denoted by g_j, and the MW drive has carrier frequency ω_0.

We evaluate and compare the two steppers discussed earlier in two aspects, the average error and the average run-time, as the number of steps is increased. The averages are taken over ten random pulses, in the form of

$$u(t) = c_1 \sin(\omega_1 t) + c_2 \cos(\omega_2 t), \tag{18}$$

where c_i's are randomly chosen from [0, 5] and ω_i's are random frequencies in $[0, 10\pi]$. The particular form of the test pulses is mainly due to the typical slow-varying modulation form of the optimal control pulses [7,20,21]. The system dynamics is numerically evolved for the total time of 0.3 μs under the application of the MW pulse. The numerical error is determined by the Hölder-∞ norm [18], quantifying the difference between the simulation results performed by TNs and a high-accuracy numerical solution based on state vector calculations. The state vector method used here exploits the Schrödinger equation numerical solver, namely *sesolve*, in the Python-based numerical library QuTiP [22]. To establish a rigorous baseline for our error estimations, we set the absolute and relative error tolerances of the solver to 10^{-12} and 10^{-10}, respectively. This forces the solver's internal error to remain strictly negligible compared to the deviations in our TN solution. We list all of the parameters used in the numerical simulations in Table I.

TABLE I. Simulation parameters. Superscripts 3 and N indicates that they are used for a system of 3 and N NV centers, respectively. Subscript i indicates that the value is the same for all NV centers. The three magnetic field parameters B_z are predeterminedly calculated to have the same resonance frequencies experimentally shown in Ref. [24], while the maximum coupling parameter g is selected.

Parameter	Value	Parameter	Value
$g_i^{(3)}$	53 kHz	$g_i^{(N)}$	100 kHz
$B_{z,1}^{(3)}$	42.82 G	$B_{z,2}^{(3)}$	88.31 G
$B_{z,3}^{(3)}$	82.88 G	$B_{z,i}^{(N)}$	65 G
$\omega_0^{(3)}$	2.797 GHz	$\omega_0^{(N)}$	2.75 GHz
γ_e	−28.025 GHz/T [23]	D	2.87 GHz [6]

Discussions. To begin with, we tested the performance of our method as the number of steps varied by fixing the system size to 3. Subsequently, we set the number of steps N_s to 1000, and varied the size of the system to evaluate the method's scalability. During the simulations, we selected the maximum bond dimension for the MPS to 3 and 16 for three and N NV centers, respectively, to keep the simulation's truncation error negligibly low.

Our numerical simulation results confirm, following our expectation, that the Simpson stepper reveals improved error rates compared to those of the Riemann stepper with only a slight increase of the run-time. Such an increase in run-time is attributed to the increase of the number of function evaluations required by the Simpson stepper. Figure 2 shows that the results for three NV centers hold for the larger system sizes with Simpson stepper yielding better error rates across all system sizes. Testing our method against the midpoint rule [25] showed mixed results, with Fig. 3 showing the Simpson stepper performing better for smaller numbers of integration steps and the midpoint stepper having slightly better performances for larger ones. A more detailed comparison with the

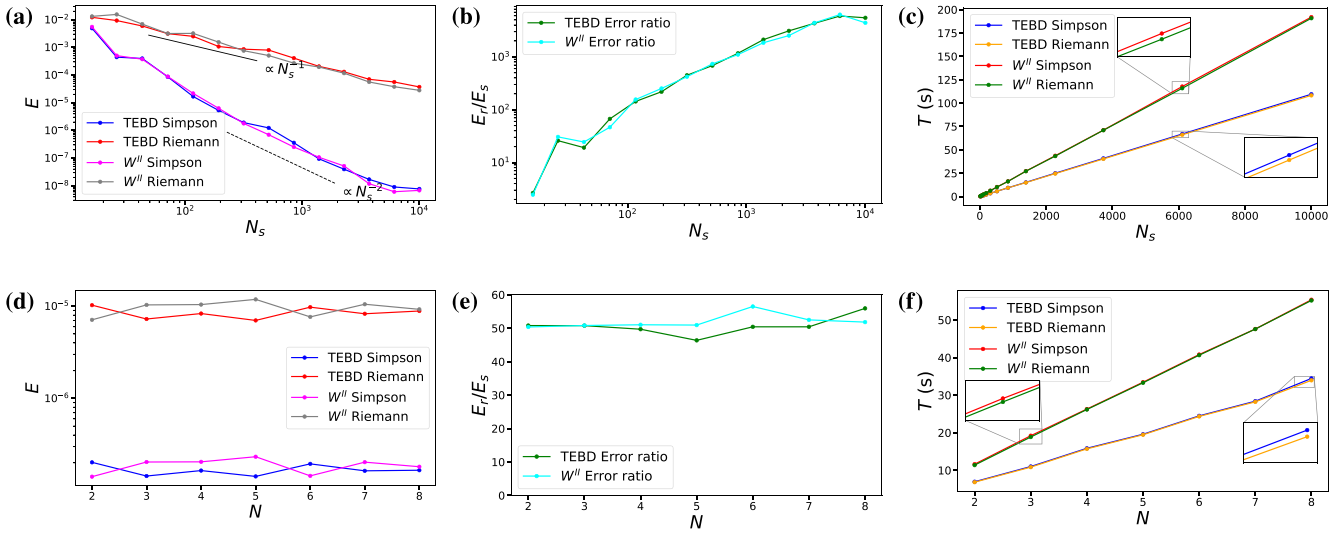


FIG. 2. Numerical performances for various system sizes of the NV spin chain. The upper panel represents the average (a) error, (b) error ratio, and (c) run-time of Riemann and Simpson steppers vs the number of integration steps N_s, for a system of three NV centers. The lower panel amounts to the corresponding quantities, as the number of NV centers N increases: (d) the average error, (e) the average error ratio, and (f) the average run-time for both steppers. The average error ratio is defined as the ratio of the average error resulting from the Riemann stepper (E_r) divided by the average error resulting from the Simpson stepper (E_s).

midpoint stepper for various system sizes, as well as results for a system of two NV centers, can be found in the Supplemental Material [26].

To sum up, we introduce a simple and practical modification to commonly used MPS time steppers for time-independent Hamiltonians by replacing the instantaneous Hamiltonian inside a single-step propagator with a Simpson-rule average of the Hamiltonian across the step. Analytically, using this averaged Hamiltonian, our proposed method restores the native third-order local accuracy of third-order-capable integrators, such as second-order TEBD and MPO W^{II}. Numerically, for the physically motivated model of driven NV centers, the Simpson stepper consistently yields a lower propagation error than that of the standard Riemann substitution across the small and intermediate system sizes, while incurring only a modest increase in run-time subject to additional Hamiltonian evaluations. When the midpoint rule is considered, our method gives superior results when the number of integration steps is small and slightly worse results for large numbers.

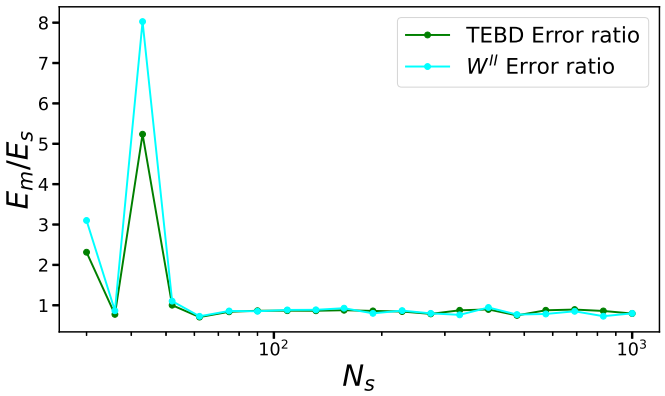


FIG. 3. Average error ratio of the midpoint stepper (E_m) and the Simpson stepper (E_s) vs the number of integration steps N_s, for a system of three NV centers.

Outlook. We conclude our Letter by outlining a few limitations and practical considerations. First, the Simpson stepper relies on the existence and boundedness of the first four derivatives of $H(t)$, for each interval, requiring those conditions to be satisfied for the method to work. Second, the method increases the number of Hamiltonian evaluations per step (i.e., two per step for the Simpson method, if we reuse the right end point in the next step), which can dramatically increase the computational costs if the time-dependent Hamiltonian $H(t)$ is expensive to construct. Finally, while our numerical calculations use a moderate maximum bond dimension to keep truncation errors negligible, large-scale many-body problems in which entanglement growth becomes significant remain limited by truncation effects. The Simpson stepper reduces the integration error; nonetheless, it does not eliminate entanglement-driven limitations. Beyond our work presented here, one can use more elaborate Magnus-based approximations with existing higher-order time-evolution algorithms for time-independent Hamiltonians to obtain more accurate approximations of the time-evolution operator. Furthermore, the adaptive time-stepping procedure can be incorporated to concentrate the computational effort for the case of rapid external driving.

Acknowledgments. We thank Jingfu Zhang, Hendry M. Lim, and Roberto Sailer for their discussions. F.J. and R.S.S. acknowledge DFG, BMBF (CoGeQ, SPINNING, QRX), QC-4-BW, Center for Integrated Quantum Science and Technology, QTBW, ERC Synergy Grant HyperQ, and EU Projects (Spinus, C-QuENS, QCircle) for their support.

All authors conceptualized the work. B.A. worked on the analytical calculations and performed numerical simulations.

B.A., J.S., and R.S.S. worked on the corresponding numerical data analyses. B.A. and R.S.S. drafted the manuscript. F.J. and R.S.S. acquired the project funding and supervised the project. All authors read and contributed to the manuscript.

Data availability. The datasets in this work are available from the corresponding author upon reasonable request. The processed data for the plots are publicly available [27].

[1] S. R. White, Density matrix formulation for quantum renormalization groups, Phys. Rev. Lett. **69**, 2863 (1992).

[2] J. C. Bridgeman and C. T. Chubb, Hand-waving and interpretive dance: An introductory course on tensor networks, J. Phys. A: Math. Theor. **50**, 223001 (2017).

[3] R. Orús, A practical introduction to tensor networks: Matrix product states and projected entangled pair states, Ann. Phys. **349**, 117 (2014).

[4] S. Paeckel, T. Köhler, A. Swoboda, S. R. Manmana, U. Schollwöck, and C. Hubig, Time-evolution methods for matrix-product states, Ann. Phys. **411**, 167998 (2019).

[5] T. Felser, Tree tensor networks for high-dimensional quantum systems and beyond, Ph.D. thesis, Universität des Saarlandes, 2021.

[6] M. W. Doherty, N. B. Manson, P. Delaney, F. Jelezko, J. Wrachtrup, and L. C. Hollenberg, The nitrogen-vacancy colour centre in diamond, Phys. Rep. **528**, 1 (2013).

[7] M. M. Müller, R. S. Said, F. Jelezko, T. Calarco, and S. Montangero, One decade of quantum optimal control in the chopped random basis, Rep. Prog. Phys. **85**, 076001 (2022).

[8] T. Oka and S. Kitamura, Floquet engineering of quantum materials, Annu. Rev. Condens. Matter Phys. **10**, 387 (2019).

[9] A. S. Santos, P. H. Pereira, P. P. Abrantes, C. Farina, P. A. Maia Neto, and R. de Melo e Souza, Time-dependent effective Hamiltonians for light–matter interactions, Entropy **26**, 527 (2024).

[10] L. Balada Gaggioli and J. Mareček, Time evolution of controlled many-body quantum systems with matrix product operators, Phys. Rev. A **112**, 062612 (2025).

[11] T. Joas, F. Ferlemann, R. Sailer, P. J. Vetter, J. Zhang, R. S. Said, T. Teraji, S. Onoda, T. Calarco, G. Genov, M. M. Müller, and F. Jelezko, High-fidelity electron spin gates for scaling diamond quantum registers, Phys. Rev. X **15**, 021069 (2025).

[12] C. L. Degen, F. Reinhard, and P. Cappellaro, Quantum sensing, Rev. Mod. Phys. **89**, 035002 (2017).

[13] O. Dhungel, T. Lenz, M. Omar, J. S. Rebeirro, M.-T. Luu, A. T. Younesi, R. Ulbricht, V. Ivády, A. Gali, A. Wickenbrock, and D. Budker, Near zero-field microwave-free magnetometry with ensembles of nitrogen-vacancy centers in diamond, Phys. Rev. B **109**, 224107 (2024).

[14] S. Blanes, F. Casas, J. Oteo, and J. Ros, The Magnus expansion and some of its applications, Phys. Rep. **470**, 151 (2009).

[15] G. Vidal, Efficient simulation of one-dimensional quantum many-body systems, Phys. Rev. Lett. **93**, 040502 (2004).

[16] M. P. Zaletel, R. S. Mong, C. Karrasch, J. E. Moore, and F. Pollmann, Time-evolving a matrix product state with long-ranged interactions, Phys. Rev. B **91**, 165112 (2015).

[17] J. Hauschild, J. Unfried, S. Anand, B. Andrews, M. Bintz, U. Borla, S. Divic, M. Drescher, J. Geiger, M. Hefel, *et al.*, Tensor network Python (TeNPy) version 1, SciPost Phys. Codebases **41** (2024).

[18] D. S. Bernstein, *Matrix Mathematics: Theory, Facts, and Formulas* (Princeton University Press, Princeton, NJ, 2009).

[19] Z. Wang, Probing surface spin interaction dynamics using nitrogen-vacancy center quantum sensors with high-fidelity state-selective transition control, Master's thesis, University of Waterloo, 2017.

[20] M. Rossignolo, T. Reisser, A. Marshall, P. Rembold, A. Pagano, P. J. Vetter, R. S. Said, M. M. Müller, F. Motzoi, T. Calarco, F. Jelezko, and S. Montangero, QuOCS: The quantum optimal control suite, Comput. Phys. Commun. **291**, 108782 (2023).

[21] H. M. Lim, G. T. Genov, R. Sailer, A. Fahrurrachman, M. A. Majidi, F. Jelezko, and R. S. Said, Efficiency of optimal control for noisy spin qubits in diamond, Phys. Rev. Appl. **24**, 054064 (2025).

[22] N. Lambert, E. Giguère, P. Menczel, B. Li, P. Hopf, G. Suárez, M. Gali, J. Lishman, R. Gadhvi, R. Agarwal, A. Galicia, N. Shammah, P. Nation, J. R. Johansson, S. Ahmed, S. Cross, A. Pitchford, and F. Nori, QuTiP 5: The quantum toolbox in Python, Phys. Rep. **1153**, 1 (2026).

[23] E. Tiesinga, P. J. Mohr, D. B. Newell, and B. N. Taylor, CODATA recommended values of the fundamental physical constants: 2018, J. Phys. Chem. Ref. Data **50**, 033105 (2021).

[24] M. Haruyama, S. Onoda, T. Higuchi, W. Kada, A. Chiba, Y. Hirano, T. Teraji, R. Igarashi, S. Kawai, H. Kawarada, Y. Ishii, R. Fukuda, T. Tanii, J. Isoya, T. Ohshima, and O. Hanaizumi, Triple nitrogen-vacancy centre fabrication by $C_5N_4H_n$ ion implantation, Nat. Commun. **10**, 2664 (2019).

[25] I. P. McCulloch, MPToolkit HOWTO: Time-dependent Hamiltonians, 2026, https://mptoolkit.qusim.net/HOWTO/TimeDependentHamiltonians.

[26] See Supplemental Material at https://link.aps.org/supplemental/10.1103/cxv4-r2bs for results for two NV centers and comparison with the midpoint stepper, which includes Refs. [6,23,25].

[27] B. Abouraya, J. Saiphet, F. Jelezko, and R. S. Said, Simulation results and plotting resources For "Efficient time-dependent dynamics of matrix product states using average Hamiltonians" [Dataset], Zenodo, 2026, https://doi.org/10.5281/zenodo.23280618.